3D3C Time-Resolved Measurements with a Single Camera Using Optical Aberrations

Rainer Hain[1], Christian J. Kähler[2]

1: Institute of Fluid Mechanics, Technical University of Braunschweig, Germany, r.hain@tu-bs.de
2: Institute of Fluid Mechanics, Technical University of Braunschweig, Germany, c.kaehler@tu-bs.de

Abstract In this contribution a simple and robust three dimensional measurement technique for the determination of all velocity components is presented. In oppositions to other techniques, only a single camera is required in order to calculate the particle positions in physical space. This is possible because the depth position of the particles is encoded by use of an optical aberration called astigmatism. The astigmatism causes the particle images to have an ellipse like shape. The length of the semi-major axis and the semi-minor axis depend on the position of the particle in depth direction.
It will be shown that this effect is well suited for decoding the particle positions. In the first section, an introduction is given and the measurement principle is shown in detail. After that, the validation of the technique is illustrated by means of synthetic generated images. Finally, experimental results are presented and a conclusion is given.

1. Introduction

In recent years, different techniques have been developed to estimate the three velocity components in a three dimensional volume. One of these methods is the particle tracking velocimetry, which allows the determination of the velocities of single particles (Virant and Dracos (1997)). A drawback of this method is the large number of cameras which is required to determine the particle positions in physical space unambiguously. Another technique is the scanning PIV (Brücker (1995), Hori and Sakakibara (2004)), where the volume is scanned with thin light sheets in order to determine the velocities in these sheets. Sometimes the in-plane velocities are measured and the third velocity component is calculated by means of mass conservation. Due to the recording of many planes, the temporal sampling of the volume is reduced which is why this method is only applicable to flows with large time scales (10 scanning sheets reduce the temporal resolution for the volume by a factor of 10). A benefit of this approach is the use of a light sheet in opposition to the other three dimensional methods which require a volume illumination. Another method for the determination of the three velocity components in a volume is holographic PIV (Barnhart et al. (1994)). This method requires a record carrier with high capacity. Using an analog medium leads to the problem of a very complicated recording and evaluation process. The application of a digital camera chip restricts the measurement volume size significantly because of the limiting pixel number.

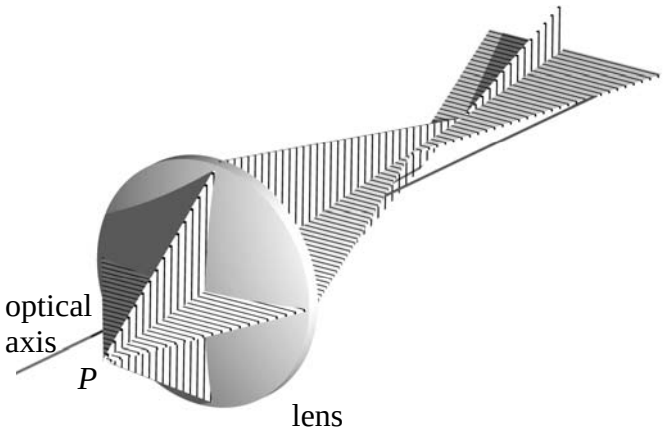

Fig. 1: Astigmatism

A relative new approach is tomographic PIV (Elsinga et al. (2005)), where a reconstruction of the measurement volume by means of tomographic algorithms is done. Similar to PTV many cameras are needed to acquire the positions of the particles in space.

As mentioned above, different problems occur when the discussed techniques are applied. One big problem is the number of

cameras which are required. This leads to high costs and often to problems with the optical access at the test facility and also to problems due to the calibration. Therefore, Willert and Gharib (1992) proposed a concept which solved most of the drawbacks of the discussed methods. Their approach is based on a single camera with a modified three hole-aperture which makes it possible to obtain three particle images from a single particle. The depth position of the particle can thus be gathered from the distances between the images. Unfortunately, the modification of the aperture and the required laser power are drawbacks of this technique.

To overcome these problems, a 3D3C time-resolved measurement technique was developed. This technique requires as well only a single camera but no modification of the aperture. The particle position in depth is encoded by means of an optical aberration, namely the astigmatism (Born and Wolf, 1980). In Fig. 1 the principle path of rays under consideration of this effect is shown. If a point light source *P* is not placed on the optical axis of a lens, there is no focal point in the image plane. Instead of one focus point, two focus lines with orthogonal orientations appear. Between these focus lines the point light source produces an ellipse like image. The size and shape of the particle image can be used to determine the three dimensional position of the particle in physical space.

2. Measurement principle

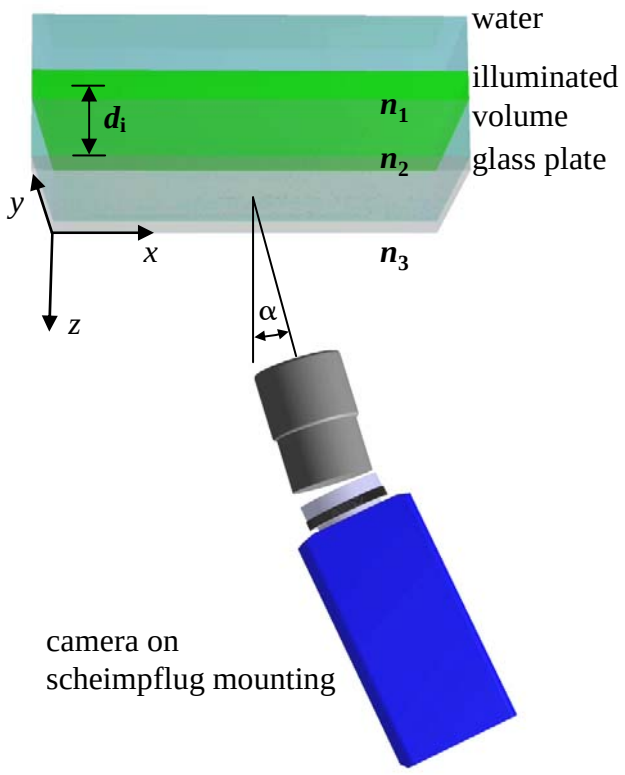

Fig. 2: Experimental setup

The astigmatism, which was mentioned before hardly occurs if objectives are used because they are corrected for optical aberrations in such a way that the aberrations are below the resolution limit of the CCD / CMOS sensors. The larger the distance of the rays of light to the optical axis, the larger are the optical aberrations such as astigmatism or coma. In order to get a well defined astigmatism, the specific setup which is shown in Fig. 2 is applied. A single camera which is mounted on a Scheimpflug adapter is aligned to the measurement volume at angle α. This angle results in combination with the refraction indices n_1, n_2 and n_3 in the astigmatism. Three exemplary images are shown in Fig. 3 where only a thin light sheet was used to illuminate the particles. This thin light sheet was traversed about 6mm towards the camera from image 1 to image 3. In the first recording, the particle images have an ellipse like shape with a small width and a large height, in the second image the width and height of the particle images is nearly equal and at the third position the width of the particle images is much larger than their height. When the whole volume is illuminated, the positions of the particles can be determined by means of their size and shape.
To estimate the positions of the particles in physical space, the following steps are necessary:

1. Calibration of the measurement volume by means of a traversed grid (similar to stereo PIV)

2. Calibration by means of thin light sheets to determine the particle shape in dependence on the position of the particle in the light sheet
3. Reconstruction of the particle position in physical space by means of the particle position on the chip, the particle shape and the calibrations mentioned above.

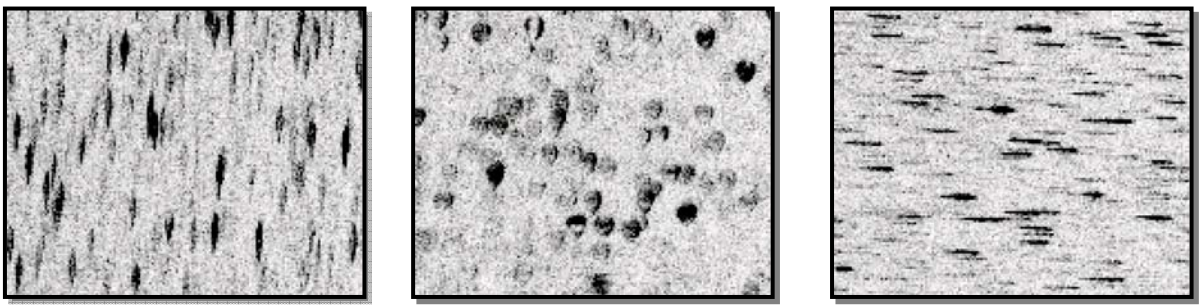

Fig. 3: Dependence of the particle image shape on the position in the measurement volume (only a thin sheet in the measurement volume is illuminated)

2.1 Measurement volume size

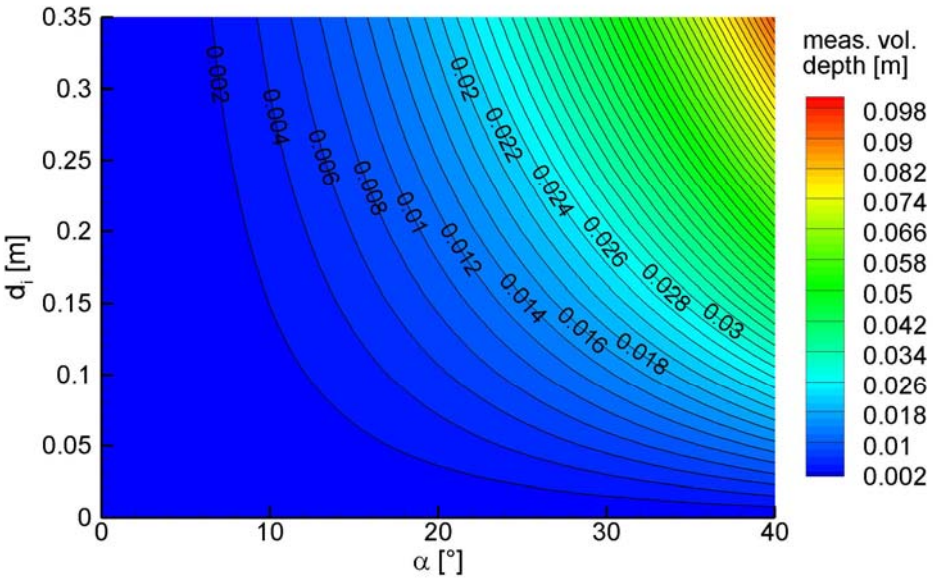

Fig. 4: The dependence of the measurement volume depth on the angle α and the distance d_i of the centre of the measurement volume to the boundary ($n_1 = n_2 = 1.33$, $n_3 = 1.0$)

The measurement volume size in *x*- and *y*-direction (assignment see Fig. 2) is mainly specified by the focal length of the objective and the distance of the objective to the measurement volume. The measurement volume depth (*z*-direction) depends on the angle α, the refraction indices n_1, n_2 and n_3 and the thickness of the glass plate. Furthermore the distance d_i from the centre of the measurement volume to the glass plate influences the measurement volume depth. If the glass plate is neglected ($n_1 = n_2$), the measurement volume depth assumes the size which is shown in Fig. 4. The calculation of this depth is done in the following way. A ray starts in the *x*-*z* plane with angle α_0 from an arbitrarily positioned point light source near the measurement volume. Because intersections of rays must be calculated later on, four additional rays are generated. Two rays (A_1 and A_2) are generated by rotating the initial ray around $\pm d\alpha_0$ in the *x*-*z* plane. The other two rays (B_1 and B_2) are generated by rotating the initial ray around $\pm d\alpha_0$ in the plane which is produced by the y-axis and the initial ray. The four rays are refracted at the intersection plane water-air. Now the intersection points of the refracted rays A_1, A_2 and B_1, B_2 are determined for $d\alpha_0 = 0$. By means of this method two virtual particle positions are calculated whose distance in *z*-direction is here assumed to be the measurement volume depth. The center between the virtual particle positions in

z-direction is d_i. In order to get a concise analytical solution for the positions of the virtual point light sources, the coordinate system given in Fig. 5 was applied. In this system, the point light source is at position

$$\begin{aligned} x_p &= -l \cdot \sin(\alpha_0) \\ z_p &= -l \cdot \cos(\alpha_0) \end{aligned} \tag{1}$$

The intersection point of the lines starting in the *x*-*z* plane is

$$\begin{aligned} x_A &= \frac{l \cdot \sin(\alpha_0) \cdot n_2^2 - l \cdot \sin^3(\alpha_0) \cdot n_1^2}{n_2^2 \cdot (\sin^2(\alpha_0) - 1.0)} \\ z_A &= \frac{l \cdot \left(n_2^2 - n_1^2 \cdot \sin^2(\alpha_0)\right)^{3/2}}{n_1 \cdot n_2^2 \cdot \left(\sin^2(\alpha_0) - 1.0\right)} \end{aligned} \tag{2}$$

The intersection point of the other two rays is

$$\begin{aligned} x_B &= -l \cdot \sin(\alpha_0) \\ z_B &= \frac{-\sqrt{n_2^2 - n_1^2 \cdot \sin^2(\alpha_0)} \cdot l}{n_1} \end{aligned} \tag{3}$$

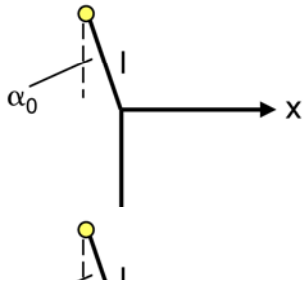

Fig. 5: Coordinate system for the calculation of the virtual point light sources

For the calculation of the values shown in Fig. 4 several angles α_0 and several distances α_0 are given to calculate the measurement volume depth. The plotted angle α is calculated by

$$\alpha = \arcsin\left(\frac{n_1}{n_2}\sin(\alpha_0)\right) \tag{4}$$

It can be seen that the measurement volume depth is adjustable in a wide range. In addition, the volume depth can be adapted by positioning high refractive materials into the beam path.

2.2 Calibration of the measurement volume

The measurement volume is viewed at angle α what leads to the distortion of the grid which is aligned parallel to the light sheet. In addition, the distortion depends on the position in the measurement volume. For this reason it is necessary to make a 3D calibration which converts the coordinates in the image plane in coordinates in physical space:

$$\begin{aligned} f(x[m]) &= f(x[px], y[px], z[m]) \\ f(y[m]) &= f(x[px], y[px], z[m]) \\ f(z[m]) &= f(x[px], y[px], z[m]) \end{aligned} \tag{5}$$

A grid is placed in the measurement volume and recorded at several positions. The intersections of

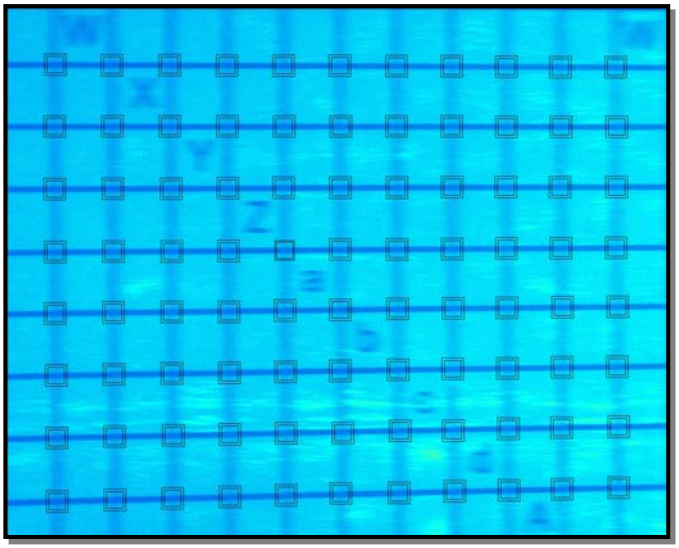

Fig. 6: Real calibration image with marked grid

the grid-lines are determined by means of cross correlation of the calibration images with an artificially generated cross. The line thickness of the cross in *x*- and *y*-direction is entered manually for each calibration position because the astigmatism causes a different line width and height for each position of calibration target in *z*-position. In Fig. 6 a real calibration image is shown where this can be seen clearly. In addition, square marks are shown. A large square means that a correlation is done at this position and a small square indicates that the correlation was successful (correlation amplitude > 0.5) and furthermore that the grid point is assumed to be valid. In the given example, the calibration target has been traversed to five positions. The original positions of the found marks are shown in Fig. 7 on the left hand side. These positions are used to calculate the fitting coefficients of a fourth order function for each direction by means of the Levenberg-Marquardt algorithm. The dewarping of the grid points with the determined coefficients leads to the positions which are shown in Fig. 7 on the right hand side. The standard deviation of these marks to the exact positions is 0.024 mm or 1.3 px (line distance in physical space is 2 mm).

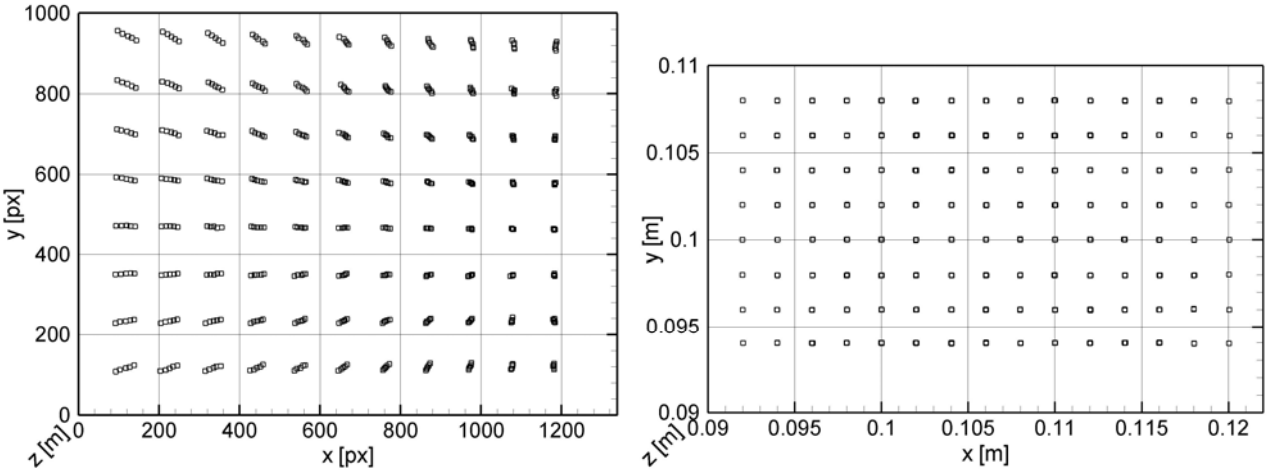

Fig. 7: Image positions of line crossing marks (left) and dewarped positions (right)

2.3 Particle image fitting

The fitting of the particle images is essential for the presented measurement technique because the particle position is directly associated with the particle image shape. Here, a 2D Gauss fit is applied:

$$f(x,y) = a_1 \cdot \exp\left(-\frac{8.0\cdot(a_2-x)^2}{a_3} - \frac{8.0\cdot(a_4-y)^2}{a_5}\right) + a_6 \qquad (6)$$

On the left hand side of Fig. 8 an original particle image is shown. At first, the pixels which might belong to a particle image are determined by means of a median filter. After that the segmentation

takes place (Fig. 8 middle) where neighboring pixels are assigned to particle images. In the next step, the pixels of a particle image in a rectangular area around the particle image are applied to fit the 2D Gauss function. The fitting is done by means of a Newton-Gauss method. In order to get a result for the fitting coefficients which does not depend on the initially chosen rectangular pixel area, 4 iterations are done. In each iteration the width and height of the area are chosen twice the width and height of the particle image (width = sqrt(a_3), height = sqrt(a_5)). The size of the area converges for most of the particle images after 2 iterations. On the right hand side of Fig. 8 the reconstructed particle image is shown which has been calculated by means of the determined coefficients.
The astigmatism causes a wave front aberration which results in the distorted particle images. Both particle image width and particle image height depend on the emitted light intensity of a particle. The emitted light intensity depends strongly on the particle size, the stability of the laser and the position of the particle in the light sheet. Hence, the particle shape is here defined by the ratio of the particle image width to the particle image height. This ratio does nearly not depend on the intensity of the emitted light of a particle and on the particle size.

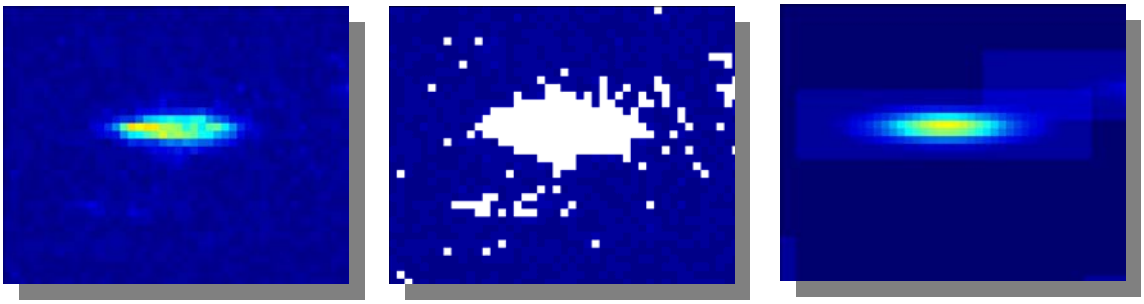

Fig. 8: Original particle image (left hand side), segmentation (middle) and reconstructed particle image (right hand side)

2.4 Calibration with particle images

Due to the astigmatism, the particle image shape depends on the positions of the particles in the depth direction (z). In addition, the particle image shape varies in x- and y-direction. For this reason a calibration

$$f\,(x[\,px], y[\,px], \textit{particle shape}) = z[m] \tag{7}$$

is necessary which maps the particle position and shape unambiguously. Therefore the measurement volume is scanned with thin light sheets and many images are recorded at every light sheet position. The particle images are extracted and fitted as mentioned in section 2.2 and for each particle image the shape parameter is calculated. This is done for the whole volume and with these extracted particle images the coefficients of the 4th order rational calibration function are determined by means of the Levenberg-Marquardt method.

3. Validation

In order to validate the presented measurement technique a simulation software for the generation of synthetic images was developed. Due to the implementation of the ray tracing technique the software allows the simulation of astigmatism. The generation of calibration grids is also possible so that the whole measurement procedure can be emulated. In Fig. 9 a result of the synthetic simulation is shown. The black points indicate the exact particle positions which are

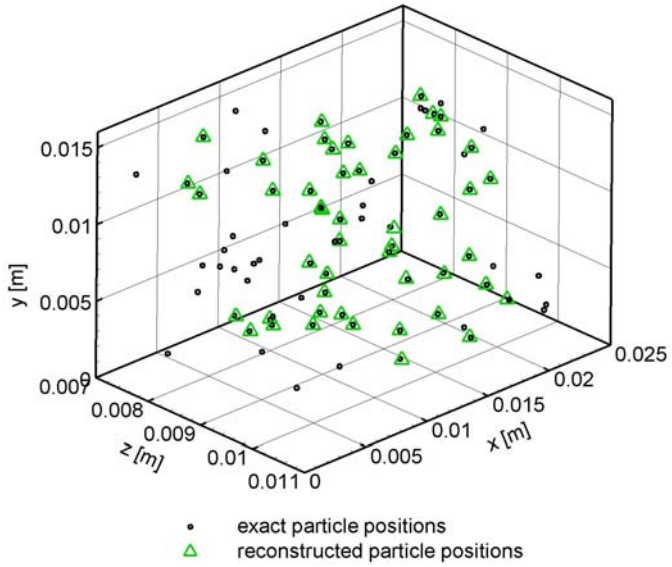

Fig. 9: Comparison of the exact and the reconstructed particle positions

known due to the simulation. The green triangles are the particle positions which have been calculated by means of the presented method. It can be seen that the agreement between these positions is quite good. In the experimental setup the particle positions are not known. However, examinations on the accuracy can be done. The calibration with particle images which was mentioned in section 2.2 is applied to experimentally recorded images in the following. In this experiment the angle α was 30° and the measurement volume depth ΔV = 15 mm. In Fig. 10 on the left hand side the particle images which are extracted from the calibration recordings are shown. The *x*- and *y*-position in the image coordinate system and the exact *z*-position in physical space are

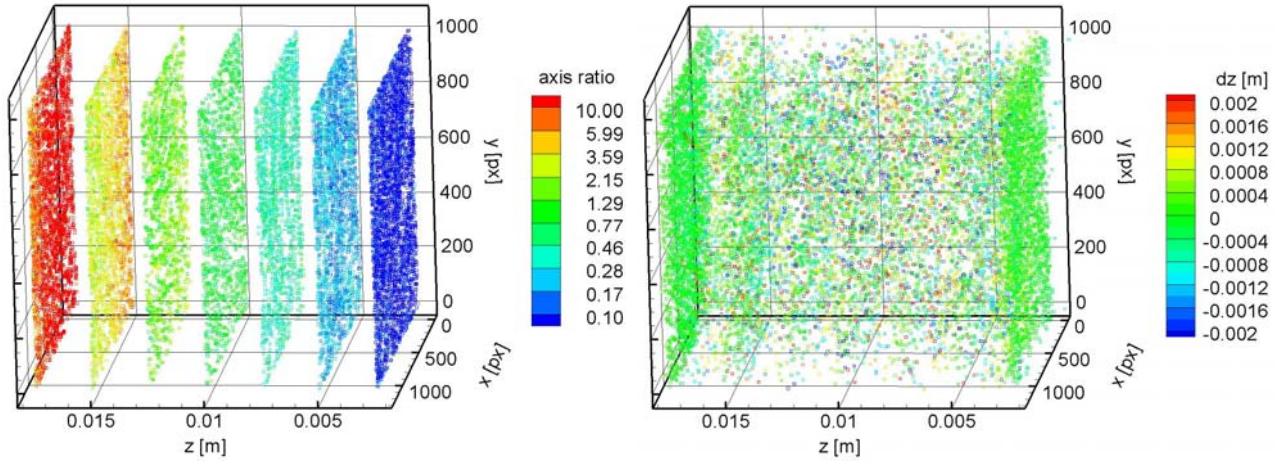

Fig. 10: The dependence of the axis ratio on the particle position (left hand side) and the deviation of the calculated z-positions to the exact z-positions (right hand side)

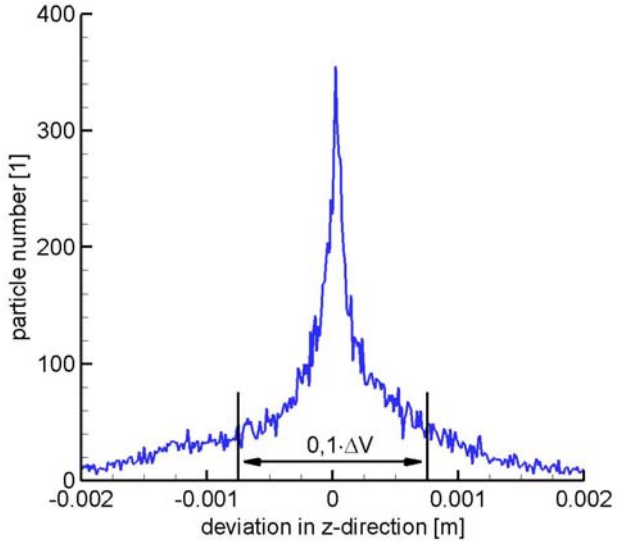

Fig. 11: PDF of the deviations in z-direction shown in Fig. 10

known. The contour color indicates the axis ratio (particle image width / particle image height). This data is used to calculate the coefficients of the calibration function for the particle images. The *z*-position can now be reconstructed by means of the positions *x* [px], *y* [px] and the axis ratio. This is given in Fig. 10 on the right hand side where the contour color indicates the deviation of the calculated *z*-position to the exact *z*-position. The PDF of this field is shown in Fig. 11. Without any postprocessing, the standard deviation in *z*-direction is 0.96 mm (6.4 % of the measurement volume depth). It can be seen that there is a clear peak at the position of 0 mm deviation in *z*-direction which means that the presented method is free of systematic errors.

4. Determination of the flow velocity

In the last sections the determination of the particle positions in physical space by means of astigmatism has been explained. However, the goal of the presented technique is the determination of the three velocity components in a volume. There are mainly two possibilities to do this. One possibility is a three dimensional correlation, similar to the PIV interrogation. Instead of interrogation windows, interrogation volumes must be applied. Because there is no more information than the particle position in the three dimensional case, a Gaussian kernel around each particle is usually positioned to allow a correlation. Besides the time consuming three dimensional correlation, another problem is the particle density which must be large enough (for the given interrogation volumes) to lead to a clear correlation peak. The sufficient size of the interrogation volumes which have to be applied for this reason can lead to a poor spatial resolution. If 1000 particle positions for example are extracted from one image and 10 particles in an interrogation volume are required to get a successful correlation, then only 100 interrogation volumes are available for the whole measurement volume. As a result, the measurement volume could be divided into 5 x 5 x 4 sub-volumes in *x*-, *y*-, and *z*-direction. Another possibility for the determination of the particle displacements is the application of a particle tracking algorithm. The uncertainty in the displacement determination will be larger than for the correlation approach but the spatial resolution will be much better. For the given example one would get 1000 displacement vectors. The decision on the suited approach for the determination of the particle displacements will be done by means of time resolved experimental data.

5. Conclusion and Outlook

The presented measurement technique can determine all velocity components in a three dimensional volume with only a single camera. Mainly for time resolved applications this is of interest because of the high costs for adequate cameras. In addition the alignment and calibration of a single camera is much easier. The measurement uncertainty of the particle position in depth direction is approximately 6.4 % of the measurement volume depth so far. In the future better suited functions for fitting the particle images shall be applied to increase the accuracy. It is assumed that this leads to an uncertainty in *z*-direction of approximately 2 %. In addition a postprocessing can be applied when the displacement of the particles is determined. This can also be used to eliminate particles whose *z*-positions have been found to be inaccurate.

6. Acknowledgements

The authors gratefully acknowledge the support of this project by the Deutsche Forschungsgemeinschaft (DFG) in the priority program 1147.

7. References

Barnhart D.H., Adrian R.J. and Papen G.C. (1994). "Phase conjugate holographic system for high resolution particle image velocimetry", Applied Optics, 33, pp. 7159 - 7170.

Born M. and Wolf E. (1980). "Principles of Optics", Pergamon Press, pp. 203 - 218.

Brücker Ch. (1995). "Digital-Particle-lmage-Velocimetry (DPIV) in a scanning light-sheet: 3D starting flow around a short cylinder", Experiments in Fluids, 19, pp. 255 - 263.

Elsinga G.E., Wieneke B., Scarano F., van Oudheusden B.W. (2005). "Assessment of Tomo-PIV for three-dimensional flows", 6th International Symposium on Particle Image Velocimetry, Pasadena, California, USA, September 21-23.

Hori T. and Sakakibara J. (2004). "High-speed scanning stereoscopic PIV for 3D vorticity measurement in liquids", Measurement Science and Technology, 15, pp. 1067 - 1078.

Virant M. and Dracos T. (1997). "3D PTV and its application on Lagrangian motion", Measurements Science and Technology, 8, pp. 1539 - 1552.

Willert C.E. and Gharib M. (1992). "Three-dimensional particle imaging with a single camera", Experiments in Fluids, 12, pp. 353 - 358.